Matter MURI, NIST, and NSF (through the Physics Frontier Center at the JQI). B.K.S. is a NIST–National Research Council Postdoctoral Research Associate. L.M.A. was supported by the NSF Graduate Research Fellowship Program. All authors except I.B.S contributed to the data collection effort. B.K.S. and L.M.A. configured the apparatus for this experiment. H.-I.L. led the team on all aspects of the edge-current and skipping-orbit measurements. H.-I.L., L.M.A., and B.K.S. analyzed data. B.K.S., H.-I.L., L.M.A, and I.B.S. performed numerical and analytical calculations. All authors contributed to writing the manuscript. I.B.S. proposed the initial experiment.

SUPPLEMENTARY MATERIALS

www.sciencemag.org/content/349/6255/1514/suppl/DC1
Materials and Methods
Supplementary Text
Fig. S1
Reference (*35*)
Database S1

9 February 2015; accepted 28 July 2015
10.1126/science.aaa8515

NANOMATERIALS

Atomically thin two-dimensional organic-inorganic hybrid perovskites

Letian Dou,[1,2]* Andrew B. Wong,[1,2]* Yi Yu,[1,2,3]* Minliang Lai,[1] Nikolay Kornienko,[1,2] Samuel W. Eaton,[1] Anthony Fu,[1,2] Connor G. Bischak,[1] Jie Ma,[2] Tina Ding,[1,2] Naomi S. Ginsberg,[1,2,4,5,6] Lin-Wang Wang,[2] A. Paul Alivisatos,[1,2,5,7] Peidong Yang[1,2,5,7]†

Organic-inorganic hybrid perovskites, which have proved to be promising semiconductor materials for photovoltaic applications, have been made into atomically thin two-dimensional (2D) sheets. We report the solution-phase growth of single- and few-unit-cell-thick single-crystalline 2D hybrid perovskites of $(C_4H_9NH_3)_2PbBr_4$ with well-defined square shape and large size. In contrast to other 2D materials, the hybrid perovskite sheets exhibit an unusual structural relaxation, and this structural change leads to a band gap shift as compared to the bulk crystal. The high-quality 2D crystals exhibit efficient photoluminescence, and color tuning could be achieved by changing sheet thickness as well as composition via the synthesis of related materials.

The organic-inorganic hybrid perovskites, especially $CH_3NH_3PbI_3$, have recently been used in solution-processable photovoltaic devices that have reached 20% power conversion efficiency (*1*–*4*). These layered materials have a general formula of $(RNH_3)_2(CH_3NH_3)_{m-1}A_mX_{3m+1}$, where R is an alkyl or aromatic moiety, A is a metal cation, and X is a halide. The variable m indicates the number of the metal cation layers between the two layers of the organic chains (*5*–*11*). In the extreme case where $m = \infty$, the structure becomes a three-dimensionally bonded perovskite crystal with a structure similar to $BaTiO_3$. In the opposite extreme where $m = 1$, the structure becomes an ideal quantum well with only one atomic layer of AX_4^{2-} separated by organic chains, in which the adjacent layers are held together by weak van der Waals forces.

This arrangement is fundamentally different from transition metal dichalcogenides, in which one layer of the metal ions is sandwiched between two hexagonal layers of S or Se atoms, affording a rigid backbone. In contrast, the layered hybrid perovskites normally have a tetragonal or orthorhombic structure and are inherently more flexible and deformable (*5*–*11*). By varying the value of m, the thickness and the related optoelectronic properties of the quantum well can be tuned. To date, many organic amines, metal cations (Cu^{2+}, Mn^{2+}, Cd^{2+}, Ge^{2+}, Sn^{2+}, Pb^{2+}, Eu^{2+}, etc.) and halides (Cl, Br, and I) have been used to construct such layered materials (m = 1 ~ 3), and their corresponding optoelectronic properties have been well studied (*12*–*15*). Previous reports have claimed that the organic layers effectively isolate the two-dimensional (2D) quantum wells in each layer from electronic coupling, if the organic chain is longer than propyl amine (*16*). This means that the properties of the atomically thin 2D quantum well should be the same as those of the bulk layered material (microscopic crystal, powder, or film). This hypothesis, as well as the technical difficulty of separating individual layers, has probably delayed investigation of free-standing single layers of such 2D materials. Very recently, attempts to obtain ultrathin 2D perovskite samples by spin coating, chemical vapor deposition, or mechanical exfoliation methods have been made with limited success (*17*–*19*).

Here we report the direct growth of atomically thin 2D hybrid perovskites $[(C_4H_9NH_3)_2PbBr_4]$ and derivatives from solution. Uniform square-shaped 2D crystals on a flat substrate with high yield and excellent reproducibility were synthesized by using a ternary co-solvent. We investigated the structure and composition of individual 2D crystals using transmission electron microscopy (TEM), energy-dispersive spectroscopy (EDS), grazing-incidence wide-angle x-ray scattering (GIWAXS), and Raman spectroscopy. Unlike other 2D materials, a structural relaxation (or lattice constant expansion) occurred in the hybrid perovskite 2D sheets that could be responsible for emergent features. We investigated the optical properties of the 2D sheets using steady-state and time-resolved photoluminescence (PL) spectroscopy and cathodoluminescence microscopy. The 2D hybrid perovskite sheets have a slightly shifted band edge emission that could be attributed to the structural relaxation. We further demonstrated that the as-grown 2D sheets exhibit high PL quantum efficiency as well as wide composition and color tunability.

A structural illustration of a monolayer 2D perovskite (Fig. 1A) shows the case with six Br atoms surrounding each Pb atom, and the four in-plane Br atoms are shared by two octahedrons, forming a 2D sheet of $PbBr_4^{2-}$. The negative charges are compensated for by the butylammonium that caps the surfaces of the 2D sheet. This structure is amenable to facile solution synthesis. The ionic character of such materials is stronger than the transition metal disulfides and diselenides, and the bulk solid is soluble in polar organic solvents such as dimethylformamide (DMF) (*20*). To grow 2D sheets, a very dilute precursor solution was dropped on the surface of a Si/SiO_2 substrate and dried under mild heating [see the supplementary materials (*21*)]. A DMF and chlorobenzene (CB) co-solvent was initially investigated, because CB helps to reduce the solubility of $(C_4H_9NH_3)_2PbBr_4$ in DMF and promote crystallization. Because CB has a similar boiling point and evaporation rate as DMF, the drying of the solvents and the crystallization process were uniform across the whole substrate.

We examined the products of this reaction by optical microscopy and atomic force microscopy (AFM), but instead of monolayers, thick particles with random shapes formed on the substrate (fig. S1). Hybrid perovskites have limited solubility in acetonitrile, and the solvent has been used previously for making microscopic hybrid perovskite single crystals (*22*). In this case, acetonitrile evaporates more quickly and helps induce the formation of the ultrathin 2D hybrid perovskite sheets. When acetonitrile was combined with DMF and CB, uniform square sheets grew on the substrate (Fig. 1B). The edge length of the square crystals ranged from 1 to 10 μm, with an average of 4.2 μm (the size distribution statistics can be found in fig. S2). The detailed synthetic procedure and discussion of the role of each solvent can be found in the supplementary text (*21*).

[1]Department of Chemistry, University of California, Berkeley, CA 94720, USA. [2]Materials Sciences Division, Lawrence Berkeley National Laboratory, Berkeley, CA 94720, USA. [3]School of Physical Science and Technology, ShanghaiTech University, Shanghai, 201210, China. [4]Department of Physics, University of California, Berkeley, CA 94720, USA. [5]Kavli Energy NanoScience Institute, Berkeley, CA 94720, USA. [6]Physical Biosciences Division, Lawrence Berkeley National Laboratory, Berkeley, CA 94720, USA. [7]Department of Materials Science and Engineering, University of California, Berkeley, CA 94720, USA.
*These authors contributed equally to this work. **†Corresponding author. E-mail: p_yang@berkeley.edu**

The thickness of the square sheets was quantified with AFM. The thickness of the crystals varied from a few to tens of nanometers; the thinnest sheets were ~1.6 nm (±0.2 nm). The AFM images of several monolayer and double-layer sheets show thicknesses of 1.6 and 3.4 nm (±0.2 nm) (Fig. 1, C and D), whereas the *d* spacing in the bulk crystal was 1.4 nm (*20*). AFM tapping mode (noncontact) was used to avoid sample damage, which can lead to a minor overestimation. For the separated monolayer, the organic chain may also relax, and the apparent thickness of the monolayer may increase slightly. Additional AFM images of other similar 2D sheets can be seen in fig. S3.

By combining AFM and optical microscopy, we correlated the appearance of the sheets in the optical image with their thickness as shown in fig. S4. The thinnest sheet on Si/SiO_2 that we could distinguish in an optical microscope was a double layer. We also prepared large single crystals of $(C_4H_9NH_3)_2PbBr_4$ and investigated the conventional mechanical exfoliation method using tape and the solvent exfoliation method using hexane to disperse the thin sheets (*23*). Unfortunately, the majority of the products from mechanical exfoliation were very thick flakes (fig. S5A) and from solvent exfoliation they were randomly shaped particles (fig. S5, B and C). The monolayer-thick particles obtained were very small (less than 1 μm), which suggests that these hybrid perovskite layers are mechanically brittle.

To determine the crystal structure of the 2D hybrid perovskites, x-ray diffraction (XRD) and TEM were used. The XRD pattern revealed that the (001) plane grew parallel to the substrate, and the out-of-plane *d* spacing was 1.42 nm (fig. S6), which is consistent with reported data for this material (*16*). The in-plane structural information was revealed by selected-area electron diffraction (SAED) in a TEM. Figure 2A shows a TEM image of a 2D sheet grown on a lacy carbon grid. After examining more than 20 individual sheets by TEM, we found that they all showed similar shape and identical diffraction patterns (additional TEM images are shown fig. S7); Fig. 2B shows the SAED pattern of another sheet. The calculated average in-plane lattice constants are a = 8.41 Å and b = 8.60 Å from five sheets, which are slightly greater than the lattice constants in the bulk crystal measured by single-crystal XRD [a = 8.22 Å and b = 8.33 Å, see (*15*) and tables S1 and S2]. The electron diffraction patterns were consistent with structural simulations, which further confirm the structure of the atomically thin 2D sheets (see figs. S8 and S9 for more discussion on the simulations/experiments on the bulk and few-layer hybrid perovskites).

We observed rapid radiation damage of the sheets under the strong electron beam. After exposing the 2D sheets to the electron beam for a few seconds, Pb was reduced and precipitated, which caused the sample to be irreversibly damaged (fig. S10). This phenomenon is similar to that observed in alkali halides (*24*). More examples of SAED patterns of individual sheets and their corresponding TEM images demonstrating the degradation can be found in fig. S11. Figure 2, C to F, shows the elemental distribution in the thin sheets; lead, bromine, carbon, and nitrogen are all present in the square.

The lattice expansion in the 2D sheets was further confirmed through macroscopic GIWAXS measurements. Figure 2G shows the GIWAXS image and Fig. 2H shows the integrated pattern. In addition, to the (200) and (020) peaks observed in TEM diffraction, many other peaks can be assigned. The *d* spacing of the (200), (020), (111), and (113) planes is 4.19 (lattice constant a = 8.38 Å), 4.25 (lattice constant b = 8.50 Å), 5.81, and 5.00 Å; respectively. These values are all greater than those of the bulk crystals and are consistent with our TEM measurements of single 2D sheets.

In addition, we examined the Raman spectra of the bulk crystal and the thin sheet as shown in fig. S12. The peaks found at 57.7 and 43.6 cm^{-1} for the bulk crystal shifted to 55.2 and 41.3 cm^{-1} for the 2D sheet, respectively. These peaks can be attributed to Pb-Br stretching and librational motions of both inorganic and organic ions (*25*), indicating that relaxation of the crystal lattice occurs in the thin sheets. Meanwhile, the peak at 122.2 cm^{-1} (from $-CH_3$ group torsional motion and insensitive to lattice distortion) did not change. The peaks for the 2D sheet became narrower, suggesting better-defined vibrational states in the thin sheet. Furthermore, our density functional theory (DFT) calculation indicates a small lattice expansion of around 0.1 Å for the monolayer as compared to the bulk $(C_4H_9NH_3)_2PbBr_4$ crystal (see the supplementary materials for details about DFT simulation).

Strong crystal lattice distortions are common for hybrid perovskites (*5*–*10*). Structural distortion–induced optical and electronic changes have been reported in bulk hybrid perovskites (*26*–*29*). Single-crystal XRD data of the bulk crystal of $(C_4H_9NH_3)_2PbBr_4$ revealed that the $PbBr_4^{2-}$ layer in the bulk crystal is highly distorted, with a

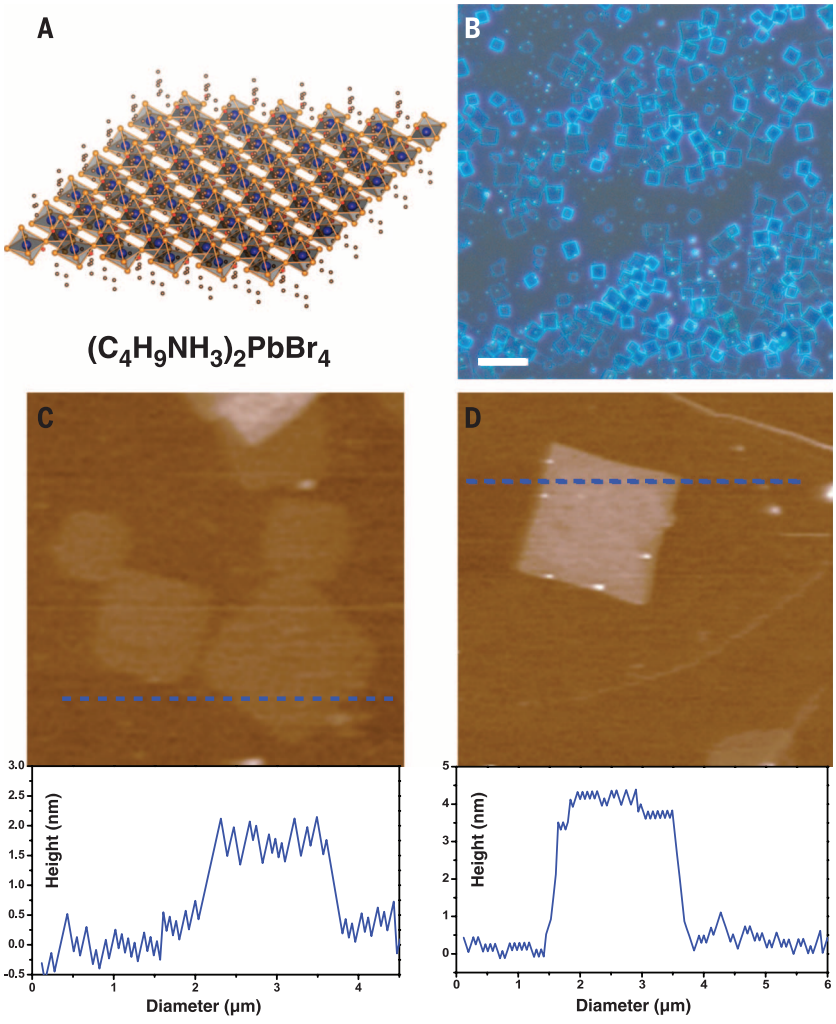

Fig. 1. Synthesis of atomically thin 2D $(C_4H_9NH_3)_2PbBr_4$ crystals. (**A**) Structural illustration of a single layer $(C_4H_9NH_3)_2PbBr_4$ (blue balls, lead atoms; large orange balls, bromine atoms; red balls, nitrogen atoms; small orange balls, carbon atoms; H atoms were removed for clarity). (**B**) Optical image of the 2D square sheets. Scale bar, 10 μm. (**C**) AFM image and height profile of several single layers. The thickness is around 1.6 nm (±0.2 nm). (**D**) AFM image and height profile of a double layer. The thickness is around 3.4 nm (±0.2 nm).

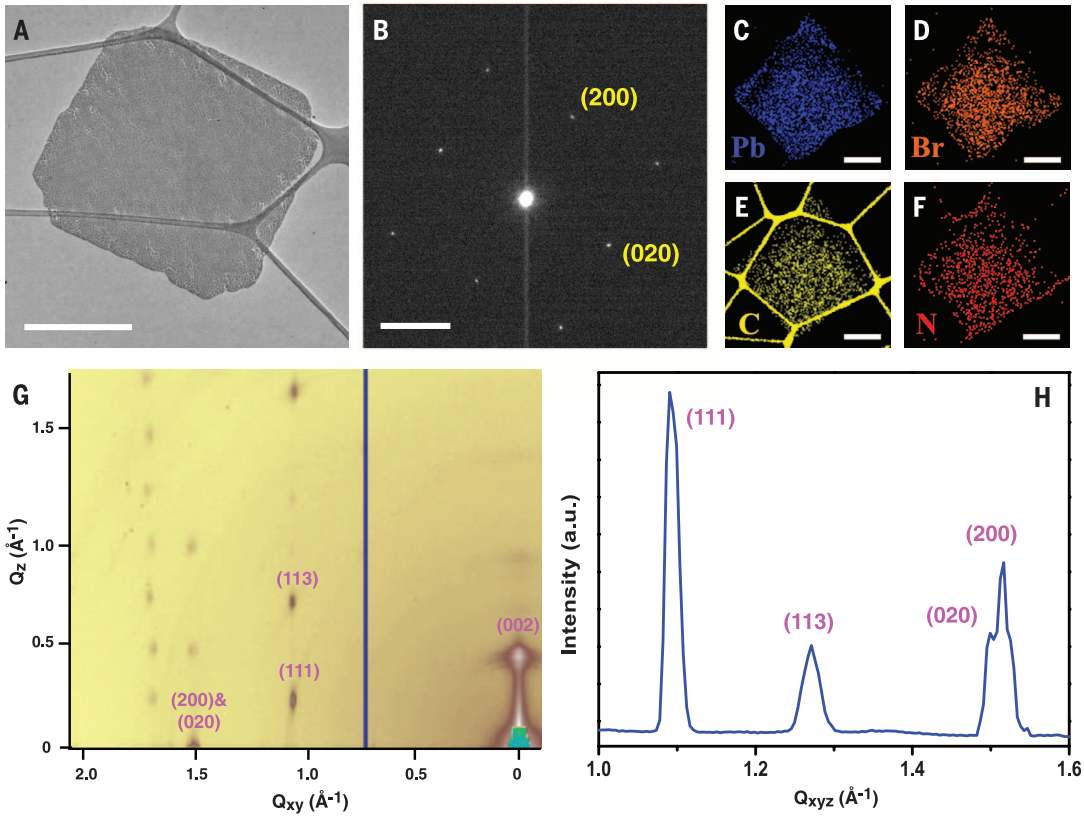

Fig. 2. TEM, EDS, and GIWAXS studies. (**A**) TEM image of a thin $(C_4H_9NH_3)_2PbBr_4$ sheet. Scale bar, 1 μm. (**B**) Electron diffraction pattern of a thin sheet of $(C_4H_9NH_3)_2PbBr_4$. Scale bar, 2 nm^{-1}. (**C** to **F**) EDS analysis showing the elemental distribution of lead, bromide, carbon, and nitrogen, respectively. Scale bars, 1 μm. (**G**) GIWAXS image of the 2D thin sheets. *Q*, wave vector in reciprocal space. (**H**) Integrated GIWAXS spectrum of the 2D thin sheets. a.u., arbitrary units.

Pb-Br-Pb bond angle of 152.94° (see fig. S13 and tables S3 and S4 for more details), which may provide driving forces for lattice relaxation in the 2D thin sheet. In other reported 2D materials, the in-plane crystal structure does not change from the bulk crystal to isolated sheets; and the optical and electronic properties change because of electronic decoupling between adjacent layers.

We investigated the PL properties of individual 2D crystals under 325-nm laser excitation. Figure 3A shows the PL spectra of the bulk $(C_4H_9NH_3)_2PbBr_4$ crystal and 2D sheets with different thickness (22, 8, and 3 layers thick, see fig. S14 for AFM images), and Fig. 3, B to E, shows the corresponding PL image of each sheet. Both the bulk materials and the sheets exhibit similar strong purple-blue light emission. The bulk crystal has an emission peak at 411 nm (2.97 eV), and the 2D sheets have slightly blue-shifted peaks at ~406 nm (3.01 eV). The slightly increased optical band gap for the ultrathin 2D sheets is probably induced by the lattice expansion. Our DFT simulation also suggests a 20-meV blue shift in PL for the single-layer 2D sheets, which is a trend consistent with the experimental observation. The 2D sheets with different thickness (from 22 to 3 layers) have similar PL spectra, the peak position shift is within 1 nm, and any lattice constant difference is within the experimental error from SAED observed between these samples. More discussion about the PL can be found in the supplementary text (*21*).

Cathodoluminescence microscopy, a technique that provides a map of the light emitted from a sample when excited by a focused electron beam with excellent lateral resolution, was used to determine the spatial distribution of emissive sites on the 2D sheets. As shown in Fig. 3G, the cathodoluminescence mapping from 395 to 435 nm shows a square shape identical to the corresponding scanning electron microscopy (SEM) images as shown in Fig. 3F, indicating that the emission is from the whole square. The PL internal quantum efficiency (QE) of the 2D sheets was estimated by comparing the integrated PL intensity (from 390 to 450 nm) of the band edge emission at room temperature (298 K) and helium cryogenic temperature (6 K), and the results are shown in Fig. 3H (*30*). There is a small red shift of the main peak from 406 to 412 nm as the temperature decreases. The emission at 421 nm (2.91 eV) at 6 K is known from the Γ_1^- state, which cannot be distinguished from the Γ_2^- state at room temperature (*26*). The PL QE for the 2D sheet is calculated to be ~26%, which is much higher than the QE of the bulk crystal (<1%), indicating the high quality of the single-crystalline 2D sheets. The PL intensity increased linearly as the excitation power increased (fig. S15), suggesting that the PL QE was constant within our measurement range. The PL lifetime of the 2D sheets was measured by time-resolved PL. As shown in Fig. 3I, the decay curve showed a bi-exponential feature with lifetimes of 0.78 ns (67%) and 3.3 ns (33%), which are near the reported data for the bulk crystals (*15*).

The chemistry of synthesizing these ultrathin 2D sheets was extended to other hybrid perovskites (*8*). We prepared $(C_4H_9NH_3)_2PbCl_4$, $(C_4H_9NH_3)_2PbI_4$, $(C_4H_9NH_3)_2PbCl_2Br_2$, $(C_4H_9NH_3)_2PbBr_2I_2$, and $(C_4H_9NH_3)_2(CH_3NH_3)Pb_2Br_7$ ultrathin 2D sheets using similar methods, and their PL spectra and optical images are shown in Fig. 4 (see fig. S16 for XRD and fig. S17 for AFM images). For the $(C_4H_9NH_3)_2PbCl_4$ sheet (i), the band edge emission was in the ultraviolet at ~340 nm, which was beyond our detection range for the single-sheet measurement. Three states in the visible region were observed at 486, 568, and 747 nm, which made the sheets appear nearly white. This emission is attributed to the transient formation of self-trapped excitons (*31*). For the $(C_4H_9NH_3)_2PbI_4$ sheet (iii), the band edge emission was at 514 nm, which is blue-shifted by 9 nm as compared to the bulk (*5*). This blue shift is consistent with the bromide case (ii) discussed above. For the chloride-bromide alloy crystal, $(C_4H_9NH_3)_2PbCl_2Br_2$ (iv), the band edge emission peak was at 385 nm, and a broad self-trapped exciton emission appeared at longer wavelength. However, the bromide-iodide alloy (v) showed only one peak at 505 nm. In the case of $(C_4H_9NH_3)_2(CH_3NH_3)Pb_2Br_7$, no well-defined squares were observed, and the thickness of the plates was ~10 nm. Preliminary PL study indicates a band edge emission at 453 nm, which is red-shifted slightly as compared to the bulk. These results indicate that the 2D hybrid perovskites have excellent composition and color tunability.

The direct growth of atomically thin sheets overcomes the limitations of the conventional exfoliation and chemical vapor deposition methods, which normally produce relatively thick perovskite plates (*17*–*19*, *32*, *33*). In contrast to other 2D materials, the structural framework of

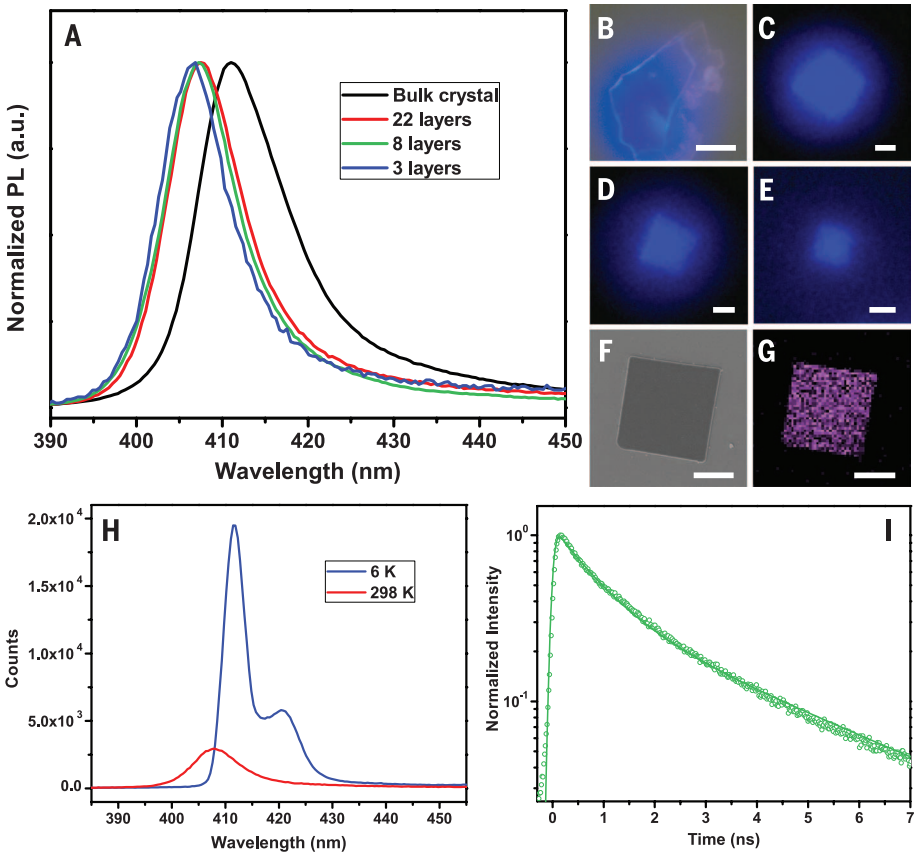

Fig. 3. PL properties of the 2D $(C_4H_9NH_3)_2PbBr_4$ sheets. (**A**) Steady-state PL spectrum of a piece of bulk crystal and several 2D sheets. (**B**) The corresponding optical image of the bulk crystal under excitation. Scale bar, 20 μm. (**C** to **E**) Optical images of the 2D sheets with 22 layers, 8 layers, and 3 layers. Scale bars, 2 μm. (**F**) SEM image of a 2D sheet. Scale bar, 2 μm. (**G**) The corresponding cathodoluminescence image showing the emission (with a 40-nm bandpass filter centered at 415 nm). (**H**) PL spectra of a 2D sheet at 298 and 6 K. (**I**) Time-resolved PL measurements showing a bi-exponential decay.

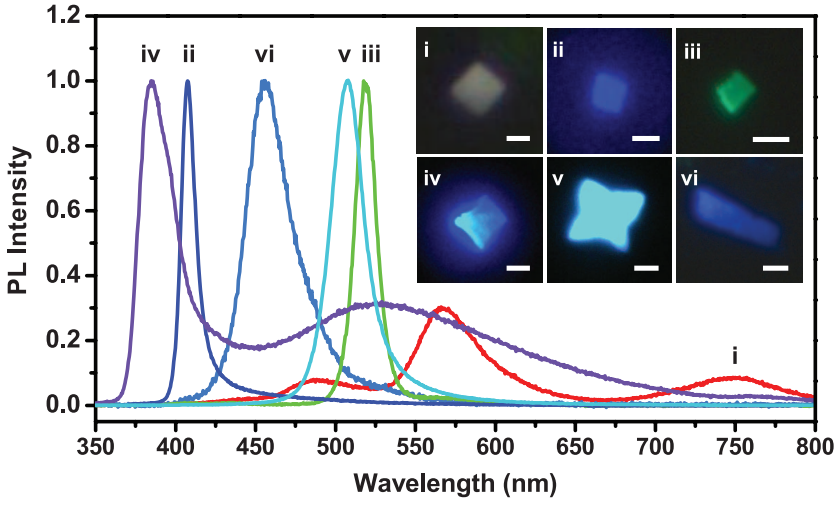

Fig. 4. Photoluminescence of different 2D hybrid perovskites. $(C_4H_9NH_3)_2PbCl_4$ (i), $(C_4H_9NH_3)_2PbBr_4$ (ii), $(C_4H_9NH_3)_2PbI_4$ (iii), $(C_4H_9NH_3)_2PbCl_2Br_2$ (iv), $(C_4H_9NH_3)_2PbBr_2I_2$ (v), and $(C_4H_9NH_3)_2(CH_3NH_3)Pb_2Br_7$ (vi) 2D sheets demonstrate that the solution-phase direct growth method is generalizable. The corresponding optical PL images are shown in the inset. Scale bars, 2 μm for (i) to (v) and 10 μm for (vi).

hybrid perovskites is flexible and deformable; and unlike the bulk crystal, the thin 2D sheets exhibit new features such as structural relaxation and PL shift. This study opens up opportunities for fundamental research on the synthesis and characterization of atomically thin 2D hybrid perovskites and introduces a new family of 2D solution-processed semiconductors for nanoscale optoelectronic devices.

REFERENCES AND NOTES

1. M. M. Lee, J. Teuscher, T. Miyasaka, T. N. Murakami, H. J. Snaith, *Science* **338**, 643–647 (2012).
2. J. Burschka *et al.*, *Nature* **499**, 316–319 (2013).
3. L. Dou *et al.*, *Nat. Commun.* **5**, 5404 (2014).
4. H. Zhou *et al.*, *Science* **345**, 542–546 (2014).
5. D. B. Mitzi, *Prog. Inorg. Chem.* **48**, 10–15 (2007).
6. G. C. Papavassiliou, *Prog. Solid State Chem.* **25**, 192–243 (1997).
7. D. B. Mitzi, *J. Chem. Soc., Dalton Trans.* **1**, 1–12 (2001).
8. G. Lanty *et al.*, *J. Phys. Chem. Lett.* **5**, 3958–3963 (2014).
9. I. Borriello, G. Cantele, D. Ninno, *Phys. Rev. B* **77**, 235214 (2008).
10. A. Meresse, A. Daoud, *Acta Crystallogr. C* **45**, 194–196 (1989).
11. T. Ishihara, J. Takahashi, T. Goto, *Solid State Commun.* **69**, 933–936 (1989).
12. R. Willett, H. Place, M. Middleton, *J. Am. Chem. Soc.* **110**, 8639–8650 (1988).
13. J. Calabrese *et al.*, *J. Am. Chem. Soc.* **113**, 2328–2330 (1991).
14. D. B. Mitzi, S. Wang, C. A. Feild, C. A. Chess, A. M. Guloy, *Science* **267**, 1473–1476 (1995).
15. N. Kawano *et al.*, *J. Phys. Chem. C* **118**, 9101–9106 (2014).
16. Y. Takeoka, K. Asai, M. Rikukawa, K. Sanui, *Bull. Chem. Soc. Jpn.* **79**, 1607–1613 (2006).
17. K. Gauthron *et al.*, *Opt. Express* **18**, 5912–5919 (2010).
18. W. Niu, A. Eiden, G. V. Prakash, J. J. Baumberg, *Appl. Phys. Lett.* **104**, 171111 (2014).
19. S. T. Ha *et al.*, *Adv. Opt. Mater.* **2**, 838–844 (2014).
20. M. A. Green, A. Ho-Baillie, H. J. Snaith, *Nat. Photonics* **8**, 506–514 (2014).
21. Materials and methods are available as supplementary materials on *Science* Online.
22. N. Mercier, S. Poiroux, A. Riou, P. Batail, *Inorg. Chem.* **43**, 8361–8366 (2004).
23. G. Cunningham *et al.*, *ACS Nano* **6**, 3468–3480 (2012).
24. L. W. Hobbs, in *Introduction to analytical electron microscopy*, J. J. Hren, J. I. Goldstein, D. C. Joy, Eds. (Plenum, New York, 1979).
25. Y. Abid, *J. Phys. Condens. Matter* **6**, 6447–6454 (1994).
26. K. Tanaka *et al.*, *Jpn. J. Appl. Phys.* **44**, 5923–5932 (2005).
27. S. Sourisseau *et al.*, *Chem. Mater.* **19**, 600–607 (2007).
28. M. R. Filip, G. E. Eperon, H. J. Snaith, F. Giustino, *Nat. Commun.* **5**, 5757 (2014).
29. E. R. Dohner, A. Jaffe, L. R. Bradshaw, H. I. Karunadasa, *J. Am. Chem. Soc.* **136**, 13154–13157 (2014).
30. D. J. Gargas, H. Gao, H. Wang, P. Yang, *Nano Lett.* **11**, 3792–3796 (2011).
31. X. Wu *et al.*, *J. Am. Chem. Soc.* **137**, 2089–2096 (2015).
32. K. S. Novoselov *et al.*, *Science* **306**, 666–669 (2004).
33. K. F. Mak, C. Lee, J. Hone, J. Shan, T. F. Heinz, *Phys. Rev. Lett.* **105**, 136805 (2010).

ACKNOWLEDGMENTS

This work was supported by the U.S. Department of Energy under contract no. DE-AC02-05CH11231 (PChem KC3103). TEM and CL characterization were carried out at the National Center for Electron Microscopy and Molecular Foundry, supported by the U.S. Department of Energy. GIWAXS measurements were carried out at beamline 7.3.3 at the Advanced Light Source, supported by the U.S. Department of Energy. X-ray crystallography was supported by NIH Shared Instrumentation Grant S10-RR027172; data collected and analyzed by A. DiPasquale. Theoretical calculation was supported by the BES/SC, U.S. Department of Energy, under contract no. DE-AC02-05CH11231 through the Material Theory program. CL characterization was supported by a David and Lucile Packard Fellowship for Science and Engineering to N.S.G. C.G.B. acknowledges an NSF Graduate Research Fellowship (DGE 1106400), and N.S.G. acknowledges an Alfred P. Sloan Research Fellowship. S.W.E. thanks the Camille and Henry Dreyfus Foundation for funding, award no. EP-14-151. M. L. thanks the fellowship support from Suzhou Industrial Park. We thank C. Zhu, C. Liu, and D. Zhang for the help with GIWAXS, AFM, and XRD measurements and H. Peng and F. Cui for fruitful discussions.

SUPPLEMENTARY MATERIALS

www.sciencemag.org/content/349/6255/1518/suppl/DC1
Materials and Methods
Supplementary Text
Figs. S1 to S17
Tables S1 to S4
References (*34*, *35*)

10 June 2015; accepted 25 August 2015
10.1126/science.aac7660

Atomically thin two-dimensional organic-inorganic hybrid perovskites

Letian Dou *et al.*

Science **349**, 1518 (2015);
DOI: 10.1126/science.aac7660